Astrophysical Phenomena Revealed by Space VLBI
H. Hirabayashi, P.G. Edwards and D.W. Murphy (eds.)

Space VLBI of Parsec–Scale Jets: the Impact of VSOP

A.P. Lobanov, J.A. Zensus, T.P. Krichbaum, & A. Witzel

Max–Planck–Institut für Radioastronomie, Auf dem Hügel 69, Bonn 53121, Germany

Abstract

Resolution improvements provided by the ongoing space VLBI mission VSOP provide an excellent opportunity for studying novel aspects of the physics of compact, parsec-scale jets in active galactic nuclei. Visibilities on space baselines contain structural information that cannot be recovered by overresolving ground array data at the same frequency. We illustrate this by discussing the results from recent VSOP observations of parsec-scale jets in 0836+710 and 3C273. For both objects, the VSOP observations have allowed to directly observe plasma instabilities developing in the jets.

1 Introduction

The VSOP (VLBI[1] Space Observatory Programme) is a Space VLBI mission utilizing worldwide arrays of radio telescopes and an orbiting 8-meter antenna deployed on the Japanese satellite HALCA[2] (Hirabayashi et al. 1998). The satellite has an elliptical orbit with apogee at 21 000 km, perigee at 560 km, and an orbital period of 6.3 hours. In each observation, the data stream from the satellite is recorded by a network of 5 satellite tracking stations, and subsequently correlated with the data from participating ground telescopes. Regular VSOP observations started in September 1997 at 1.6 and 5 GHz. We compare here the properties of space and ground VLBI images obtained from two 5 GHz VSOP observations of compact extragalactic jets in 0836+710 and 3C 273.

2 VSOP and Ground VLBI Images

The VSOP observations were made in October (0836+710) and December (3C 273) of 1997. Basic description of the observations is given in

[1] Very Long Baseline Interferometry
[2] Highly Advanced Laboratory for Communication and Astronomy

Table 1: Summary of the VSOP observations

	Ground Array	B [MHz]	$N_{\rm ch}$	$t_{\rm obs}$ [hrs]	$t_{\rm gs}$ [hrs]	$uv_{\rm gg}$ [Mλ]	$uv_{\rm gs}$ [Mλ]
(1)	(2)	(3)	(4)	(5)	(6)	(7)	(8)
0836+710	VLBA	32	512	11.4	5.2	2–142	180–550
3C 273	VLBA+EB	32	256	12.5	6.7	2–137	100–535

Column designation: 2 – supporting ground VLB array; 3 – bandwidth; 4 – number of spectral channels; 5 – total observing time; 6 – observing time with ground–space baselines; 7,8 – uv–ranges on ground–ground and ground–space baselines.

Table 2: Parameters of the images of 0836+710

Image	$S_{\rm tot}$	$S_{\rm max}$	$S_{\rm min}$	$\sigma_{\rm RMS}$	$D^{\rm peak}_{\rm rms}$	Beam
(1)	(2)	(3)	(4)	(5)	(6)	(7)
VLBA	2.167	0.918	−0.001	0.2	4600:1	2.2, 1.5, 30.8
VSOP	2.156	0.432	−0.003	0.5	900:1	0.9, 0.3, −36.3
HALCA	0.731	0.325	−0.007	1.4	200:1	0.7, 0.2, −36.9

Column designation: 2 – total CLEAN flux [Jy]; 3 – peak flux density [Jy/beam]; 4 – lowest negative flux density [Jy/beam]; 5 – RMS noise [mJy/beam]; 6 – peak-to-RMS dynamic range; 7 – restoring beam: major axis, minor axes [mas], position angle of the major axis [deg].

Table 1. The data were correlated at the NRAO VLBA[3] correlator in Socorro NM, USA. For each source, we have produced three different images: a) ground array image (VLBI image) using only ground–ground baselines, b) space baseline image (HALCA image) with only ground–space baselines included, and c) VSOP image using the entire dataset. The respective images of 0836+710 are shown Figure 1. Table 2 compares the properties of all three images of 0836+710. The relative changes of restoring beam sizes and dynamic ranges are similar in the respective images of 3C 273 (Lobanov et al. 2000). Discussions on more specific details of imaging and properties of the images can be found elsewhere (Lobanov et al. 1998, 1999, 2000).

[3]The Very Long Baseline Array of the National Radio Astronomy Observatory. The NRAO is a facility of the National Science Foundation operated under cooperative agreement by Associated Universities, Inc.

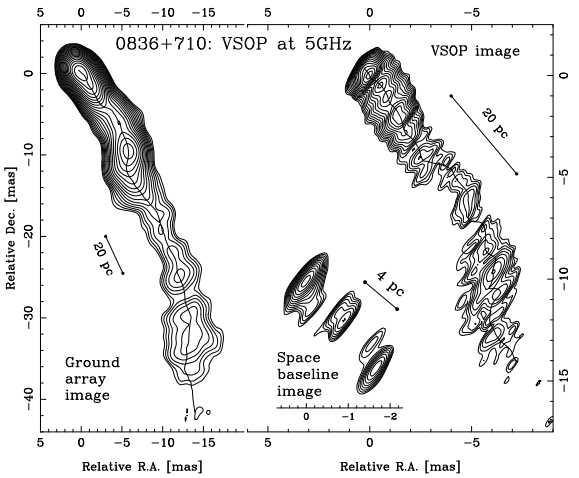

Figure 1: Ground array, VSOP, and space-baseline–only images of 0836+710 (Lobanov et al. 1998). Linear scales are given for $H_0 = 100\,\mathrm{km\,s^{-1}\,Mpc^{-1}}$ and $q_0 = 0.5$. In the ground array and VSOP images, the jet ridge line is marked. The space baseline image is obtained using only the baselines to HALCA. All structures seen in this image are consistent with those found in both the VSOP and ground array images. The contour levels are drawn as follows: -0.9, $0.9{\times}2^{n/2}$ mJy/beam in the ground array image; -2, $2{\times}2^{n/2}$ mJy/beam in the VSOP image; -5, $5{\times}1.5^{n}$ mJy/beam in the space baseline image. Other parameters of the images are given in Table 2

3 Impact of Improved Angular Resolution

3.1 0836+710: Plasma Instabilities in the Jet

The VSOP image of 0836+710 allows us to study the jet morphology and physical conditions on linear scales up to 1 kpc. We have shown that, on the scales of $\lesssim 700h^{-1}$ pc, the curved ridge line of the jet can be modelled by a pressure confined relativistic outflow with Lorentz factor $\gamma_\mathrm{j} \approx 11$, Mach number $M_\mathrm{j} \sim 6$, and opening half-angle $\phi_\mathrm{j} \approx 1^\circ$ (Lobanov et al. 1998). In this description, the two main factors responsible for the observed curvature of the jet ridge line are: 1) Kelvin-Helmholtz instabilities developing in the jet plasma and 2) variations of the angle, θj, between the velocity vector of the outflow and the line of sight. The derived variations of θ_j are consistent with the observed variable apparent speeds along the jet.

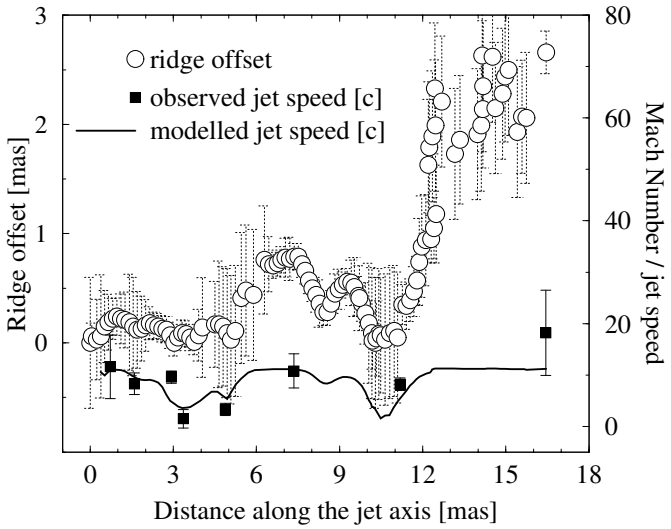

Figure 2: Relation between the ridge line and observed jet speeds in 0836+710 (Lobanov et al. 1998). Circles are measured offsets of the jet ridge line from the jet axis at P.A.$= -146°$; squares denote speeds reported by Otterbein (1996) at different locations in the jet; solid line represents apparent speed variations derived from the measured ridge line offsets, for a jet with Mach number, $M_{\rm j} = 6$, Lorentz factor, $\gamma_{\rm j} = 11$, and opening half-angle, $\phi_{\rm j} = 1°$.

The derived $\theta_{\rm j}$ changes smoothly between 3° and 65°, with largest values occurring at ~ 3 mas and ~ 10 mas distances — which are incidentally the locations where the most pronounced lateral displacements are reported (Otterbein 1996). The predicted $\beta_{\rm app}$ (plotted in Figure 2 with the solid line) is in a good agreement with the measured jet speeds. We would like to emphasize that the achieved consistency between the model and observed speeds is preserved, if the chosen direction of the jet axis are within a few degrees from the one we have used. In that case, only the derived jet Mach number would have differed from $M_{\rm j} = 6$ obtained above. Sparsity of the available speed measurements precludes better kinematic modelling and selecting the jet axis unambiguously. We expect that making such a selection would require determining the continuous velocity distribution along the jet, for which a suitable monitoring program should be designed, aimed at obtaining a sequence of high dynamic range and high fidelity VLBI images of the source.

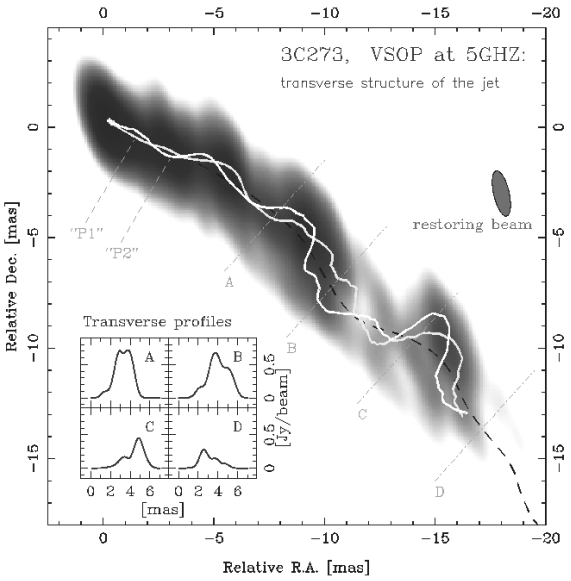

Figure 3: The 5 GHz VSOP image of the parsec-scale radio jet of 3C273 (Lobanov et al. in preparation – see also Color Figure 6). The image has a restoring beam is 2.09×0.70 mas at P.A.= 12.9° and a peak flux density of is 4.52 Jy/beam. The dashed black line is the smoothed ridge line of the jet. The dot-dashed white lines denote the locations of the 4 flux density profiles shown in the inset. It is possible to identify two internal emitting features (denoted P1 and P2) responsible for the observed transverse brightness distribution in the jet. The locations of these features are marked in the image by the grey lines. These features can be represented by Kelvin–Helmholtz instabilities developing in a relativistic plasma.

3.2 3C273: Transverse Structure of the Jet

The VSOP image of 3C 273 offers an even more striking example of the effect of improved angular resolution (Lobanov et al. 2000). The transverse emission distribution in the jet of 3C 273 shows remarkable deviations from a Gaussian shape, owing to the favorable orientations of the space baselines which provide a 0.7 mas resolution in the direction perpendicular to the jet axis. This is particularly visible in the emission profiles taken across the jet (Figure 3).

The ground VLBI image also resolves the jet transversely, and suggests possible edge brightening. However, only with the improved res-

olution of the VSOP image, it becomes possible to assess the true complexity of the transverse structure of the jet, with up to three emission components across the jet (i.e. in panel B in Figure 3). The stronger central component often dominates the profiles, possibly masking the presence of the third emitting feature. With the existing data, we are able to recover the locations of the two stronger emitting features (denoted P1 and P2, in Figure 3) inside the jet of 3C273. The locations of these features reveal remarkably regular, oscillating patterns which can be reconciled with the presence of Kelvin–Helmholtz instabilities developing and propagating in the relativistic plasma of the jet. We are able to obtain the wavelengths and amplitudes of at least 4 different modes of the instabilities, thereby for the first time establishing directly their presence in the jet. The measured parameters of the instabilities represent the transverse structure of the jet on scales of up to 20 milliarcseconds (~ 40 parsecs).

4 Conclusion

The discussed VSOP observations of 0836+710 and 3C 273 show that space VLBI arrays containing a fast–orbiting satellite element provide an excellent opportunity for high-resolution and high dynamic range imaging of parsec–scale jets in extragalactic objects, and open up new opportunities for studies of physical processes in relativistic plasmas observed in extragalactic jets.

Acknowledgements. We gratefully acknowledge the VSOP Project, which is led by ISAS in cooperation with many organizations and radio telescopes around the world.

References

Hirabayashi, H., Hirosawa, H., Kobayashi, H. et al. 1998, *Science*, **281**, 1825 and erratum **282**, 1995

Lobanov, A.P., Krichbaum, T.P., Witzel, A., et al. 1998, *A&A*, **340**, 60

Lobanov, A.P., Krichbaum, T.P., et al. Witzel, A., & Zensus, J.A. 1999, *NewAR*, **43**, 741

Lobanov, A.P., Zensus, J.A., Abraham, Z., et al. 2000, *Adv. Sp. Res.*, **26**, 669

Otterbein, K. 1996, PhD thesis, Univ. of Heidelberg